Influence of noncondensable gases on thermodynamic control on-ground experiments using a substitute fluid

Samuel Mer, Jean-Paul Thibault, Christophe Eric Corre

Influence of Noncondensable Gases on Thermodynamic Control On-Ground Experiments Using a Substitute Fluid

Samuel Mer[1]
Institut de Mecanique des Fluides de Toulouse,
UMR5502—CNRS and INPT and UPS,
Toulouse 31000, France
e-mail: samuel.mer@imft.fr

Jean-Paul Thibault
LEGI Laboratory—UMR5519,
Univ. Grenoble Alpes and CNRS,
Grenoble 38000, France
e-mail: jean-paul.thibault@legi.cnrs.fr

Christophe Corre
LMFA Laboratory—UMR 5509,
Ecole Centrale de Lyon and CNRS,
Ecully 69134, France
e-mail: christophe.corre@ec-lyon.fr

A cryogenic propellant submitted to heat load during long duration space missions tends to vaporize to such an extent that the resulting pressure rise must be controlled to prevent storage failure. The thermodynamic vent system (TVS), one of the possible control strategies, has been investigated using on-ground experiments with NOVEC$_{1230}$ as substitution fluid. Results obtained for self-pressurization (SP) and TVS control phases have been reported in a previous work. The unexpected inverse thermal stratification observed during these experiments is analyzed in the present work and related to the influence of noncondensable gases. Noncondensable gases, present inside the tank in the form of nitrogen—ten times lighter than the substitution fluid vapor—generate a concentration stratification in the ullage. Assuming the NOVEC$_{1230}$ remains at saturation in the whole ullage, the density stratification which results from this concentration stratification can explain the observed inverse thermal stratification. [DOI: 10.1115/1.4037449]

1 Introduction

Future operations in space exploration require the ability to store cryogenic liquids for long duration. Residual heat loads, due to sun or heat conduction in the launcher structure, induce cryogenic propellant vaporization and tank self-pressurization (SP). Due to the extended duration of the mission, an un-controlled tank self-pressurization may lead to storage failure.

The thermodynamic vent system (TVS) control strategy originally proposed in Ref. [1] has been recently investigated in the literature both numerically [2–4] and experimentally [5]. A schematic view of a tank control with a TVS system is presented in Fig. 1. The TVS strategy relies on the following key ideas: thanks to a liquid acquisition device (see Ref. [6] for more details), some liquid propellant is pumped from the tank to a heat exchanger in order to be cooled down. This subcooled liquid fraction is re-injected inside the tank as a jet or a spray in both vapor and liquid phases. In order to create the heat exchanger cold source (heat sink), another liquid fraction is withdrawn from the tank (vented branch), expanded through a Joule–Thomson valve, and thus cooled down. Once used as the cold source, this liquid fraction is vented out of the tank as a vapor phase and lost for the mission (excepting the use of the venting thrust). The subcooled injection is followed by a vapor condensation and a liquid bath destratification which tends to depressurize the tank.

Recently, Mer et al. [5] published an on-ground experimental study of a TVS system using NOVEC$_{1230}$ as substitution fluid. Issues with the management of thermal boundary conditions, which were reported in previous work by Barsi and Kassemi [7] and Demeure [8], were successfully solved thanks to the development of an active insulation technique yielding a net zero heat flux wall boundary condition. The influence on SP and TVS control dynamics of control parameters such as tank filling, tank heat load, injection mass flow rate, and injection temperature was analyzed in Ref. [5] through a series of experiments which also provide a useful database for the validation of numerical models.

[1]Corresponding author.

However, an unexpected inverse thermal stratification of the ullage was observed in Ref. [5] during tank SP experiments. The present contribution provides a detailed analysis of this stratification taking into account the presence of noncondensable gases (namely, nitrogen) in the experimental facility. The observed inverse thermal stratification can be explained by the concentration stratification of noncondensable gas in the ullage.

First, the experimental apparatus is briefly presented in Sec. 2 along with its instrumentation, the fluid purity assessment, and the experimental procedure leading to thermal stratification measurements. A model is described and applied in Sec. 3 to explain the unexpected inverse thermal stratification measured in the SP experiment from the presence of noncondensable gas in the tank. The influence of thermal boundary forcing and subcooled

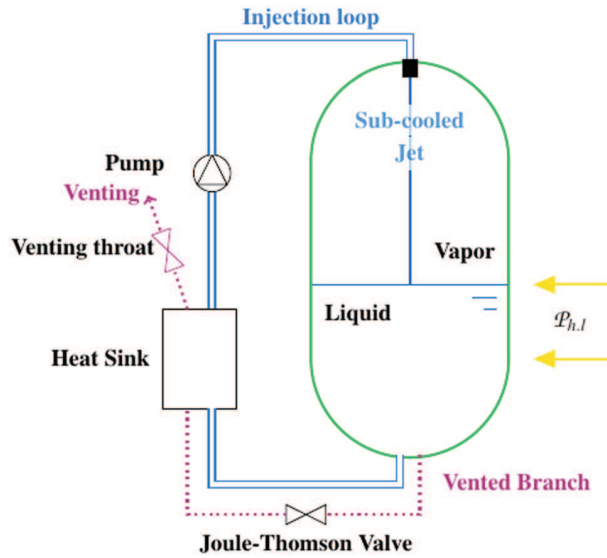

Fig. 1 Schematic view of a TVS controlled tank. The injection loop drives directly a subcooled jet inside the ullage. The vented branch creates the cold source heat sink.

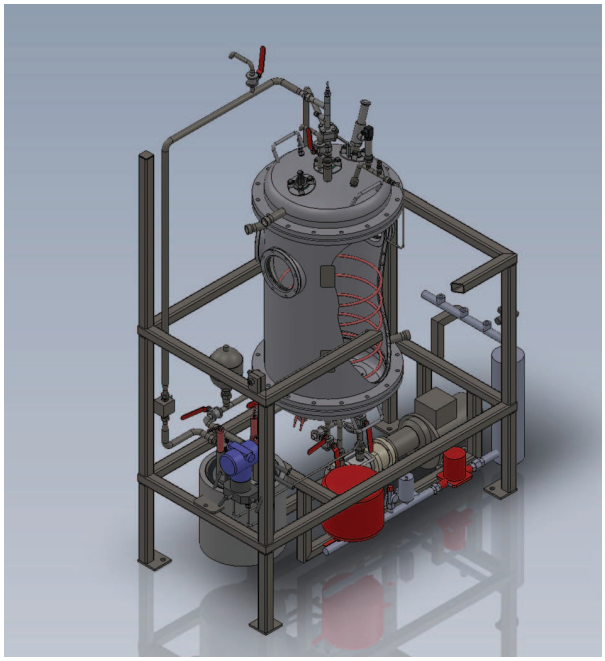

Fig. 2 Partially flayed computer-aided design view of the experimental apparatus

injection on the concentration stratification of noncondensable gas is discussed, respectively, in Secs. 4 and 5.

2 Experimental Apparatus

The SP and TVS experiments make use of a 110 L tank displayed in Fig. 2. The $NOVEC_{1230}$ retained as substituent fluid enable to perform these experiments close to room temperature, since its saturation temperature at atmospheric pressure is such that $T_{sat_{NOVEC_{1230}}}(p_{atm}) = 50\,^{\circ}C$ [9].

2.1 Active Thermal Insulation Technique. An active insulation technique provides an accurate management of the wall boundary condition—the tank walls are thermalized by a water loop circulating inside a double envelope (see in Fig. 3). The envelope temperature regulation set-point $T_{env_{SP}}$ is prescribed with a multi-proportional–integral–derivative (PID) technique so as to follow the average temperature inside the tank T_{ave} plus a compensation factor ε counter-balancing the thermal losses occurring by natural convection inside the experimental room

$$T_{env_{SP}} = T_{ave} + \varepsilon \tag{1}$$

The tank average temperature is defined as

$$T_{ave} = \frac{\sum_{sens.} \rho_i(T_{sensor}) \cdot c_{p,i}(T_{sensor}) \cdot T_{sensor}}{\sum_{sens.} \rho_i(T_{sensor}) \cdot c_{p,i}(T_{sensor})}, \quad i \in [vap, liq] \tag{2}$$

with $c_{p,i}(T_{sensor})$ the heat capacity of the sensor phase (either liquid or vapor). The compensation factor is computed as

$$\varepsilon = 9.4\,e-3 \times (T_{env_{WP}} - T_{amb}) \tag{3}$$

where the current envelope temperature working-point $T_{env_{WP}}$ is estimated by using the temperature measured by four sensors (see Fig. 3)

$$T_{env_{WP}} = \frac{1}{6} \cdot \left(3 \cdot T_{env_{in}} + T_{env_{out_1}} + T_{env_{out_2}} + T_{env_{out_3}}\right) \tag{4}$$

while the experimental room temperature T_{amb} is estimated as

$$T_{amb} = \frac{1}{3} \cdot (T_{amb1} + T_{amb2} + T_{amb3}) \tag{5}$$

The tank heat load $\mathcal{P}_{h.l.}$ can be either directly imposed by an electrical heating coil immersed in the liquid bath or its effect can be accounted for by adding a wall thermal imbalance constant $\Delta T_{h.l.}$ to the envelope regulation set-point of the active insulation technique

$$T_{env_{SP}} = T_{ave} + \varepsilon + \Delta T_{h.l.} \tag{6}$$

When using the electrical coil, the tank heat load $\mathcal{P}_{h.l.}$ equals the electrical power delivered by the coil and can be directly obtained from the data processing unit. Alternatively, when the wall thermal imbalance technique is used, a post-processing of the

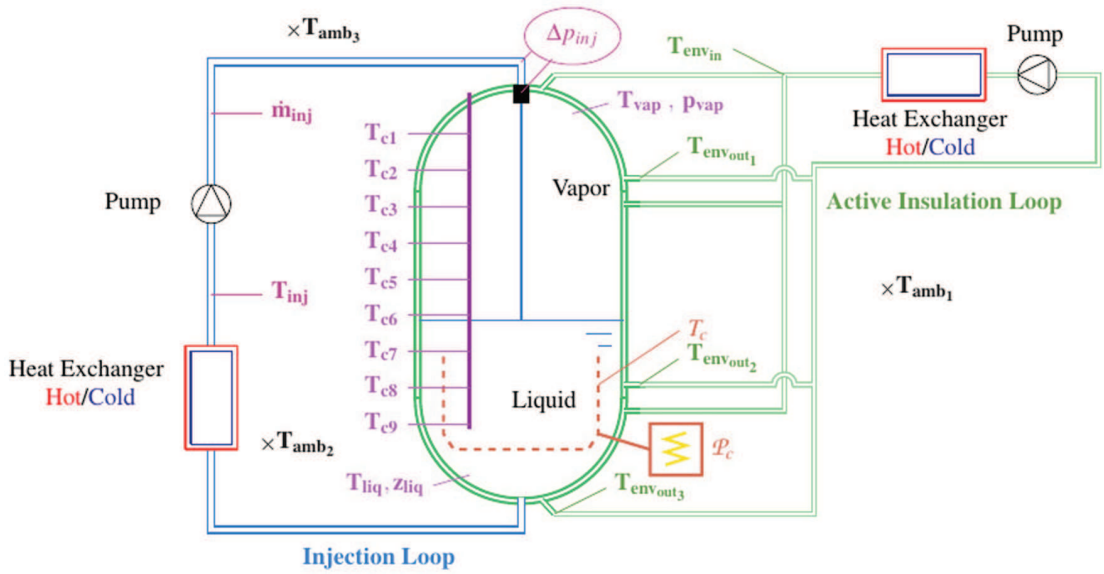

Fig. 3 Schematic view of the experimental facility with its instrumentation, injection loop, and double envelope active insulation loop

experimental self-pressurization rate is required to derive $\mathcal{P}_{\text{h.l.}}$. Considering the experimental initial filling $\mathcal{F}$, an iterative procedure relying on the homogeneous thermodynamic model presented in Ref. [4] determines the tank heat load $\mathcal{P}_{\text{h.l.}}$ which corresponds to the observed experimental self-pressurization rate.

During TVS control experiments, the injection loop (see in Fig. 3) is activated so that liquid is withdrawn from the tank, at a fixed mass flow rate $\dot{m}_{\text{inj}}$, and subcooled in a heat exchanger before being re-injected, at a fixed temperature T_{inj}, into the ullage.

2.2 Instrumentation. The experimental facility instrumentation is sketched in Fig. 3. A multisensor temperature probe, made of nine PT100 (1/10th of class B) sensors regularly spaced along the vertical, gives access to the thermal stratification along a vertical line located approximately at $R_{\text{tank}}/2$ from the tank axis of symmetry. Other control sensors give, respectively, access to the tank filling $\mathcal{F}$, the injection mass flow rate $\dot{m}_{\text{inj}}$, the injection temperature T_{inj}, the pressure drop through the injector Δp_{inj}, the vapor pressure p_{vap}, the vapor temperature T_{vap} at the top of the tank and the liquid temperature T_{liq} at the bottom of the tank, the double envelope water circuit temperatures $T_{\text{env,in}}$, $T_{\text{env,out1}}$, $T_{\text{env,out2}}$, and $T_{\text{env,out3}}$, and the ambient temperatures T_{amb1}, T_{amb2}, and T_{amb3}. A temperature sensor is fastened to the heating coil T_{coil} to measure the eventual temperature imbalance induced by the heat power supply. The acquisition chains are identical for all the temperature sensors. The PT100 sensors are connected to a data recorder of Versadac$^{\text{TM}}$ Eurotherm type which converts the sensors analogical signal into a numerical one and communicates by Ethernet with two controllers (Nanodac$^{\text{TM}}$ Eurotherm). Each controller manages a PID control loop (see injection loop and active insulation loop in Fig. 3). The controllers are connected to a computer where the control loops are set up and the PID parameters are tuned. The whole temperature acquisition chain has been calibrated to minimize the measurement error ($\Delta T \approx \pm 0.05\,^{\circ}\text{C}$). The measurement error associated to the vapor pressure sensor is $\delta P \approx \pm 5 \times 10^3\,\text{Pa}$.

2.3 Fluid Purity Assessment. Since the physical phenomenon under study should be ideally a single species problem involving only the liquid propellant and its vapor, it is essential to ensure the fluid purity in the experimental tank in order to remain representative of the real system. Note, for instance, that Bullard [10] showed the presence of noncondensable gases significantly increases the characteristic cooling time of a TVS control phase.

Flow purity is assessed by comparing the measured p_{vap} with the saturation pressure extrapolated from the interface temperature $p_{\text{sat}}(T_{\text{inter}})$. In the present experiments, this extrapolation is based on the physical properties of NOVEC$_{1230}$ (Clausius–Clapeyron saturation equation [9]). Due to the residual content of noncondensable gases and fluid impurities (the fluid has an industrial grade corresponding to a 99% purity), a perfect agreement between the measured p_{vap} and $p_{\text{sat}}(T_{\text{inter}})$ is never reached in the experiments. The observed pressure offset $p_{\text{vap}} - p_{\text{sat}}(T_{\text{inter}})$ corresponds to the partial pressure of noncondensable gases p_{noncond}. For all the results presented in this work, the partial pressure of noncondensable gases in the tank always remains below $9.0 \times 10^3\,\text{Pa}$, which corresponds to a molar fraction value of noncondensable gases below 7%. For safety reason and to prevent oxidation, the NOVEC$_{1230}$ containers are pressurized with nitrogen during shipping. Furthermore, in order to transfer the fluid from the shipping containers to the experimental facility, the containers are pressurized with nitrogen. From now on, the noncondensable gases are assumed to be exclusively nitrogen. A purification procedure has thus been developed to purify the NOVEC$_{1230}$ by venting out the noncondensable gas/nitrogen. Its main steps are the following ones: (1) the tank is filled until overflowing by a top drain-cock; (2) thanks to the envelope temperature regulation, the temperature inside the tank is prescribed to $T_{\text{ave}} = 50\,^{\circ}\text{C}$; (3) the drain-cock located at the top of the tank allows to impose the atmospheric pressure inside the tank so that the fluid is brought to saturation since for NOVEC$_{1230}$ $T_{\text{sat}}(1\,\text{bar}) = 50\,^{\circ}\text{C}$; and (4) since the solubility of noncondensable gases tends to zero when the fluid is close to saturation, noncondensable gases can be vented out by the top drain-cock. Other purification techniques have been presented in the literature. Barsi [11] uses an iterative void pumping method yielding noncondensable molar fraction levels below 5%, which is slightly better than the levels obtained in the present study. This iterative void pumping method is however much more complex and expensive than the purification method proposed here. More importantly, a 5% molar fraction of noncondensable gases has still a significant impact on the tank temperature stratification so that it is anyway relevant to observe and analyze the noncondensable gas influence on the temperature vertical distribution.

2.4 Experimental Procedure. For SP experiments, the temperature and pressure linearly increase in the tank due to the heat power supply. The initial condition of a self-pressurization is a fixed average temperature ($T_{\text{ave}} = 55\,^{\circ}\text{C}$ in the following analysis), and the stopping criterion is a prescribed average temperature ($T_{\text{ave}} = 60\,^{\circ}\text{C}$ in what follows). The slope of the linear pressure rise, with respect to time, depends on the tank heat load $\mathcal{P}_{\text{h.l.}}$ and the initial tank filling $\mathcal{F}$.

Temperature distributions are measured in the tank using the previously described instrumentation for two distinct SP experiments using the same initial liquid filling $\mathcal{F} = 66\%$ but two different thermal heat loads, namely, $\mathcal{P}_{\text{h.l.}} = 26$ W and $\mathcal{P}_{\text{h.l.}} = 52$ W, both delivered by the electrical heating coil. The measured thermal stratification is displayed in Fig. 4 for both experiments at two different self-pressurization times corresponding to the same average temperature $T_{\text{ave}} = 57.5\,^{\circ}\text{C}$ in the sense of Eq. (2). This average temperature level is reached after 4.15 h (respectively, 2.06 h) for $\mathcal{P}_{\text{h.l.}} = 26$ W (respectively, $\mathcal{P}_{\text{h.l.}} = 52$ W). As expected, Fig. 4 displays a quite homogeneous temperature distribution in the liquid bath, due to a high thermal diffusivity of the phase. However, the temperature distribution in the vapor exhibits an unexpected behavior, since a quasi-linear temperature decrease from the interface to the ullage top is observed. Such a linear temperature decrease in the vapor phase is systematically observed during all the performed SP experiments. This decrease actually

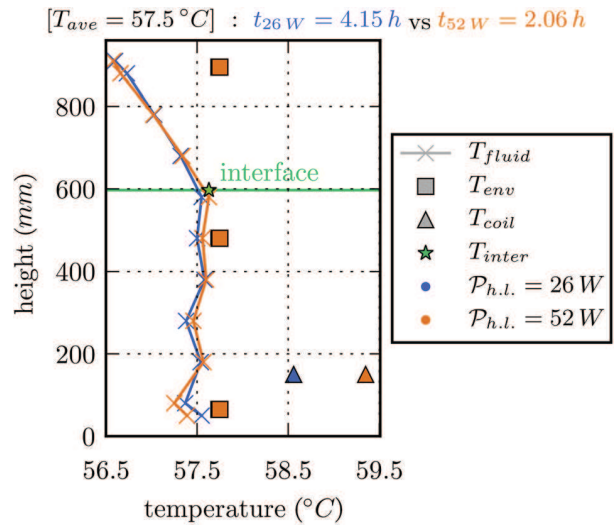

Fig. 4 Vertical temperature distribution in the fluid (the interface separates the two phases: ullage on top of the liquid bath), heating coil temperature, and wall temperature (double envelope) during a self-pressurization phase and for two different heat loads, $\mathcal{P}_c$ both for $T_{\text{ave}} = 57.5\,^{\circ}\text{C}$

corresponds to the inverse of the expected thermal stratification. The experiment fulfills a condition of quasi-equilibrium, due to its very slow dynamics—the rate of the average temperature rise is about 1 °C h^{-1}—so that no subcooled vapor should appear in the tank. Considering a pure $NOVEC_{1230}$ vapor ullage for a given pressure, the hot vapor is lighter than the cold one and should thus be located at the tank top, yielding a regular rise of the vapor temperature from the interface to the tank top.

A steady analysis performed for a plateau temperature of 55 °C shows that this linear temperature decrease in the vapor phase goes on steadily in the tank even when the average temperature remains constant. This observation allows to exclude a cold point at the top of the tank for being the cause of the unexpected thermal stratification. The inverse ullage thermal stratification is explained in Sec. 3 by taking into account the presence of noncondensable gas in the tank.

3 Influence of Noncondensable Gas Concentration on Thermal Stratification

The nitrogen gas contained inside the experimental tank is assumed to behave like an ideal gas, with its density derived from the usual equation of state

$$\rho_{\mathrm{vap}_{N_2}} = \frac{p_{\mathrm{tot}}}{\frac{R}{M_{N_2}} \cdot T} = \frac{p_{\mathrm{tot}}}{r_{N_2} \cdot T} \tag{7}$$

with $r_{N_2} = 296\ \mathrm{J\,kg^{-1}\,K^{-1}}$ the nitrogen gas constant. The $NOVEC_{1230}$ saturated vapor density is derived from the fluid properties tables, provided by 3M [9], and computed using the following temperature-based expression:

$$\rho_{\mathrm{sat}_{NOVEC_{1230}}} = 4.6843 \times 10^{-3} \times T^2 - 3.0367 \times 10^{-2} \times T + 2.9735 \tag{8}$$

with T in °C.

The nitrogen gas density, at the operating temperature and pressure, is about $1.4\ \mathrm{kg\,m^{-3}}$, yielding a density ratio with the $NOVEC_{1230}$ vapor higher than 10. This high density ratio can be identified as the source of a concentration stratification in the ullage.

A simple model was developed in order to explain the observed inverse thermal stratification from the concentration stratification of noncondensable gas. Assuming that the ullage total pressure is uniform (i.e., neglecting the hydrostatic pressure in the ullage) and that the $NOVEC_{1230}$ vapor remains at saturation in the whole ullage, the $NOVEC_{1230}$ and nitrogen partial pressure distributions in the ullage are computed as

$$\begin{cases} p_{NOVEC_{1230}} = p_{\mathrm{sat}_{NOVEC_{1230}}}(T) \\ p_{N_2} = p_{\mathrm{tot}} - p_{NOVEC_{1230}} \\ p_{\mathrm{tot}} = p_{\mathrm{vap}} \end{cases} \tag{9}$$

The molar fraction distributions for nitrogen and $NOVEC_{1230}$ are immediately obtained from

$$\begin{cases} x_{NOVEC_{1230}} = \dfrac{p_{NOVEC_{1230}}}{p_{\mathrm{vap}}} \\ x_{N_2} = \dfrac{p_{N_2}}{p_{\mathrm{tot}}} \end{cases} \tag{10}$$

Finally, the apparent ullage density can be computed from Eqs. (7), (8), and (10) using an ideal mixture law

$$\rho_{\mathrm{ave}} = x_{NOVEC_{1230}} \times \rho_{\mathrm{sat}_{NOVEC_{1230}}} + x_{N_2} \times \rho_{N_2} \tag{11}$$

This type of analysis is applied to the temperature profile presented in Fig. 4 for the $\mathcal{P}_{\mathrm{h.l.}} = 52$ W experiment. Note that the $\mathcal{P}_{\mathrm{h.l.}} = 26$ W case yields similar results, not reported here to preserve the clarity of the figures. The relationships (9) are applied for each point of the temperature distribution displayed in Fig. 4 and also recalled in the left picture of Fig. 5 in order to obtain the partial pressure distributions in the vapor. From the partial pressure distributions, the molar fraction distributions are computed from Eq. (10) and plotted on the central picture in Fig. 5. The density is finally obtained from Eq. (11) and reported on the right picture in Fig. 5.

It can be observed that the nitrogen molar fraction remains between 4% and 7%—this finding is consistent with the fluid purity assessment reported in Sec. 2.3—and rises from the interface to the ullage top. Moreover, the computed vertical distribution of density agrees well with a natural stratification condition, where the lighter fluid remains above the heavier one. The inverse thermal stratification can thus be explained by the presence of nitrogen in the experimental tank. The high density ratio between nitrogen and $NOVEC_{1230}$ generates a nitrogen concentration

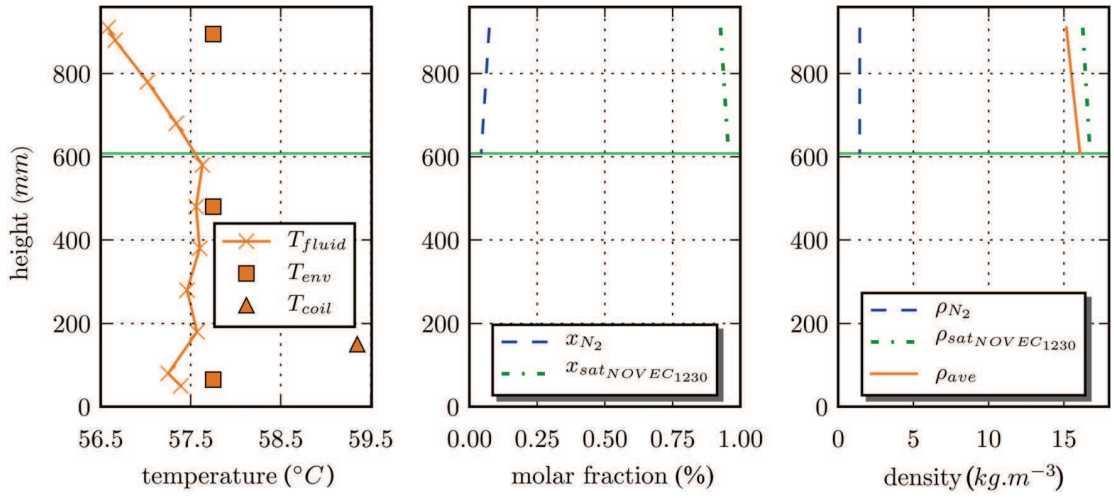

Fig. 5 ***Inverse*** **thermal stratification analysis during SP and more particularly for the SP experiment presented in Fig. 4 for $\mathcal{P}_{\mathrm{h.l}} = 52$ W: temperature, molar fraction of each component, and density vertical distributions in the ullage (above the interface)**

stratification in the ullage. The $NOVEC_{1230}$ at saturation in the ullage adapts its temperature to the partial pressure of $NOVEC_{1230}$, which diminishes from the interface to the ullage top, yielding a linear decrease of the ullage temperature from the interface to the ullage top.

4 Influence of Thermal Boundary Conditions on Stratification

To assess the influence of thermal boundary conditions on the temperature stratification, two self-pressurization experiments have been performed with the same initial tank filling ($\mathcal{F}$) and tank heat load ($\mathcal{P}_{\text{h.l.}}$). However, the two distinct strategies, described in Sec. 2.1, are used to prescribe the tank heat load. The first SP experiment is such that a wall thermal imbalance or wall heating $\Delta T_{\text{h.l.}} = 0.66\,^{\circ}\text{C}$ is imposed. The post-processing algorithm mentioned in Sec. 2 yields the corresponding tank heat load, namely, $\mathcal{P}_{\text{h.l.}} = 42.5$ W. The second SP experiment is performed for the same tank heat load but directly delivered this time by the electrical heating coil, with the joint use of the net zero heat flux wall boundary condition as done in the experiments reported in Sec. 3. The average temperature rise in the tank during both experiments is displayed in Fig. 6. The very good agreement between both strategies, as far as tank average temperature is concerned, demonstrates that the post-processing algorithm used to derive the tank heat load $P_{\text{h.l.}}$, corresponding to a given value of $\Delta T_{\text{h.l.}}$, is working well. Let us now investigate in more detail the vertical temperature distribution in the tank, available from the multisensor temperature problem described in Sec. 2.2.

The vertical temperature profiles measured in both experiments for the same value of the average temperature, namely, $T_{\text{ave}} = 57.5\,^{\circ}\text{C}$, are displayed in Fig. 7 along with the corresponding envelope temperature T_{env} and heating coil temperature T_{coil}.

The coil heating case displays a slight overheating of the liquid phase compared to the wall heating case. At the very bottom of the tank, one can notice in fact a slight overheating of the wall heating case with respect to the coil heating case. This behavior can be explained considering that the bottom temperature sensor is located in the vicinity of the tank envelop and is thus slightly affected by the wall thermal imbalance constant $\Delta T_{\text{h.l.}}$. The heating coil temperature is in fact about 1.5 °C warmer than the average liquid bath temperature. Despite the high thermal diffusivity of the liquid phase, the thermal imbalance induced by the heating coil leads to a slight local overheating of the liquid phase. The ullage temperature displays a quasi-linear temperature decay from the interface to the ullage top as previously observed in Fig. 4.

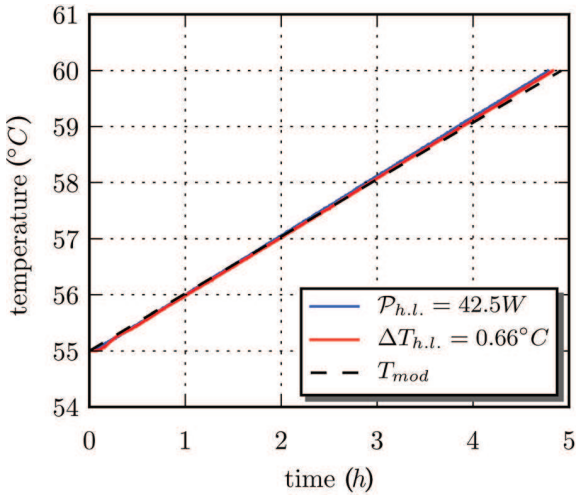

Fig. 6 Influence of the heating mode on the temperature evolutions inside the tank during SP experiments with a tank filling of 66% and a fixed tank heat load of $\mathcal{P}_{\text{h.l.}} = 42.5$ W imposed by the two strategies presented in Sec. 2.1. The dashed line represent the model prediction.

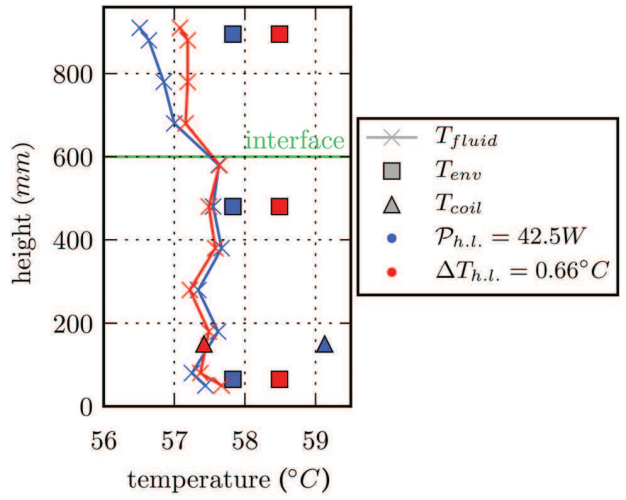

Fig. 7 Influence of the heating mode on the temperature vertical distribution inside the tank during SP experiments with a tank filling of 66% for an average temperature of 57.5 °C and a tank heat load of $\mathcal{P}_{\text{h.l.}} = 42.5$ W

The wall heating case shows first that the coil temperature sensor (displayed as a triangle) behaves like a passive temperature sensor in the liquid bath, since there is no longer a thermal power delivered by the heating coil. The envelope temperature, represented by squares, displays the 0.66 °C prescribed temperature gap and highlights the influence of $\Delta T_{\text{h.l.}}$ on the envelope regulation temperature process with respect to the coil heating case. It is observed that the ullage thermal stratification is significantly different from the one observed for the coil heating case. The wall thermal forcing heats up the ullage and modifies the nitrogen molar fraction stratification previously observed in Fig. 5. The nitrogen molar fraction and density distribution associated with the wall heating case are presented in Fig. 8, following the computation process described in Sec. 3. It appears once again that the vertical *inverse* thermal stratification is due to a nitrogen concentration stratification in the ullage. The latter is itself dependent on the tank thermal forcing mode. The self-pressurization experiments are performed in a closed tank, so that the total nitrogen mass in the tank is kept constant. This total mass is divided into two parts: one part is dissolved in the liquid bath, while the other, present in the ullage, is mixed with the vapor. The distribution of the nitrogen total mass between these two parts depends on the thermal forcing in such a way that the $NOVEC_{1230}$ vapor remains at saturation in the ullage. In order to better apprehend the thermal forcing dependency of the nitrogen total mass distribution, a TVS control experiment is analyzed in Sec. 5. The TVS experiment consists in injecting in the ullage a highly subcooled liquid jet (initially $\Delta T = 20\,^{\circ}\text{C}$) at a fixed massflow rate and temperature. The thermal equilibrium in the tank is thus strongly destabilized when the injection starts. The experiment ends, typically after $\approx$ 5–7 h, when the tank returns to thermal equilibrium, so that the jet cooling power $\mathcal{P}_{\text{jet}}$ (see Eq. (12)) balances the tank heat load $\mathcal{P}_{\text{h.l.}}$.

5 Subcooled Jet Influence on Ullage Gas Concentration

The nitrogen molar fraction along the ullage vertical is computed using the methodology described in Sec. 3. This vertical

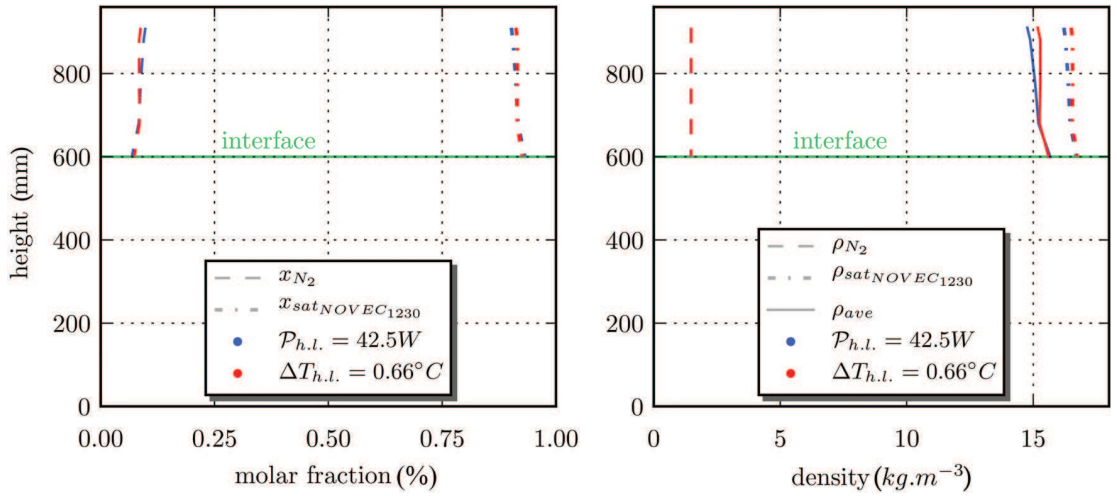

Fig. 8 Influence of the heating mode on the ullage thermal stratification analysis for the SP experiments presented in Fig. 7. Left: ullage components average molar fractions. Right: ullage components average density.

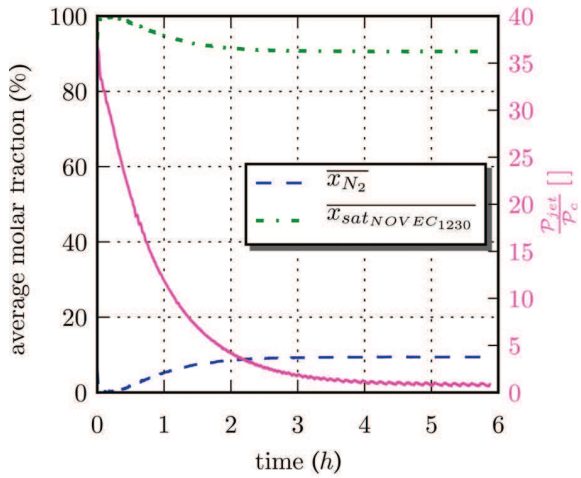

Fig. 9 Evolution of the components average molar fraction in the ullage and evolution of the thermal power ratio during a TVS control experiment such that $T_{inj} = 40\,°C$, $\dot{m}_{inj} = 43\,g\,s^{-1}$, $\mathcal{F} = 66\%$, and $\mathcal{P}_c = 26$ W

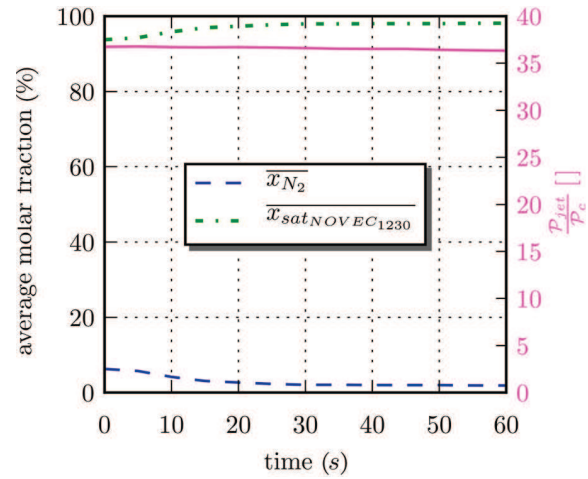

Fig. 10 Zoom on the first minute of the TVS experiment presented in Fig. 9

distribution can be averaged in order to derive the components average molar fractions $\overline{x_{N_2}}$ and $\overline{x_{sat_{NOVEC_{1230}}}}$, whose evolution during a TVS control experiment can then be plotted. Such an evolution of average molar fractions in the ullage is displayed in Fig. 9 for a TVS control experiment performed with the following control parameters: $T_{inj} = 40\,°C$, $\dot{m}_{inj} = 43\,g\,s^{-1}$, $\mathcal{F} = 66\%$, and $\mathcal{P}_{h.l.} = 26$ W delivered by the heating coil. The evolution of the TVS control thermal power ratio $\mathcal{P}_{jet}/\mathcal{P}_{h.l.}$ is also reported in Fig. 9, with $\mathcal{P}_{jet}$ the cooling power of the subcooled jet expressed as

$$\mathcal{P}_{jet} = \dot{m}_{inj} \cdot c_p(T_{inj}) \cdot (T_{ave} - T_{inj}) \tag{12}$$

This power ratio has to remain above unity for the TVS regulation to be efficient [4]. It drops during the TVS experiment following the average temperature decrease. In the present analysis, the thermal power ratio is used as a nondimensional measure of the thermal imbalance induced by the subcooled jet during a TVS experiment.

It can be observed in Fig. 9 that the nitrogen average molar fraction collapses at the beginning of the TVS experiment, as soon as the subcooled jet enters the ullage. The average molar fraction $\overline{x_{N_2}}$ collapses from 6% to ≈0.0% in less than 25 s after the injection start as depicted in Fig. 10.

To explain this trend, one can examine the thermal power ratio keeping in mind that the higher this ratio the more subcooled the entering jet. Subcooling the jet drives the liquid away from the tank saturation conditions. It subsequently induces the condensation of the $NOVEC_{1230}$ present in the ullage. Moreover, the saturation concentration of nitrogen dissolved in the liquid bath of $NOVEC_{1230}$ increases when the temperature decreases. Since the liquid present in the incoming jet is originally withdrawn from the liquid bath of the tank, the dissolved nitrogen concentration in this liquid fraction originally equals the one of the liquid bath. However, after being subcooled in the heat exchanger and reinjected inside the tank, its relative concentration is smaller and undersaturated because, as usual, the saturated concentration in the liquid increases when temperature decreases. Consequently, the subcooled jet tends to absorb nitrogen more avidly than the rest of the liquid contained in the tank. This is the source of a mass transfer of nitrogen from the ullage to the subcooled jet. A quantification of the saturation concentration of nitrogen in both the liquid and the vapor of $NOVEC_{1230}$ was intended. To the best of the author's knowledge, the only available values of Henry's law constant for $NOVEC_{1230}$ are unfortunately out of range of the pressure and temperature operating conditions in the present

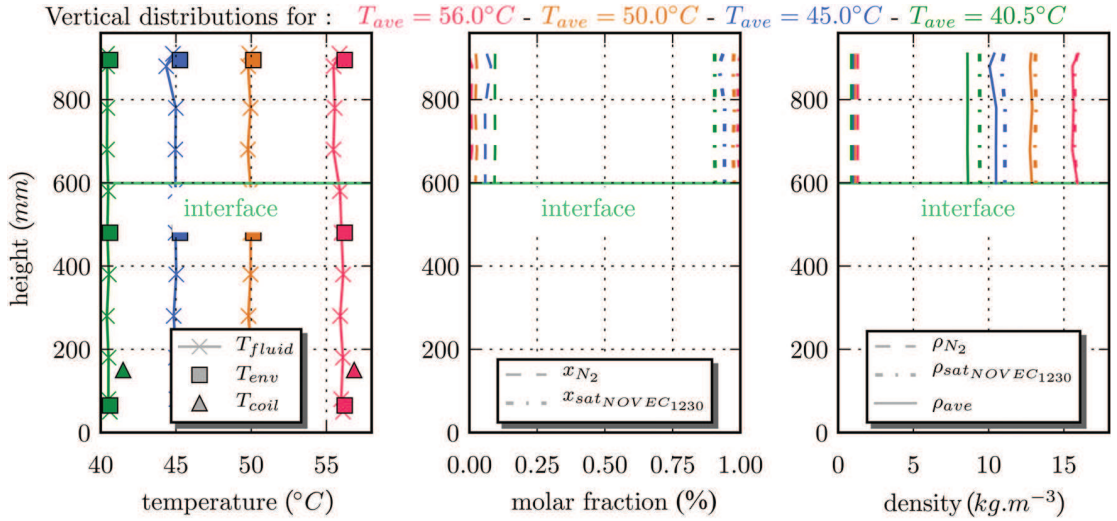

Fig. 11 Subcooled injection influence on ullage average molar fractions and density vertical distributions during a TVS control experiment such that $T_{inj} = 40\,°C$, $\dot{m}_{inj} = 43\ g\,s^{-1}$, $\mathcal{F} = 66\%$, and $\mathcal{P}_{h.l.} = 26\ W$

Table 1 Data summary for the ullage stratification analysis

Self-pressurization—$T_{ave} = 57.5\,°C$

Case				T_{sensor} (°C)		x_{N_2} (%)		$x_{NOVEC_{1230}}$ (%)		ρ_{N_2} (kg m^{-3})		$\rho_{sat_{NOVEC_{1230}}}$ (kg m^{-3})		ρ_{ave} (kg m^{-3})	
$\mathcal{F}$	$\mathcal{P}_{h.l.}$	Method	$\Delta T_{h.l.}$	Min	Max	Min	Max	Min	Max	Min	Max	Min	Max	Min	Max
66	52	Coil	—	56.58	57.55	4.34	7.32	92.7	95.7	1.43	1.47	16.25	16.62	15.16	16.08
66	42.5	Coil	—	56.51	57.57	6.64	9.82	90.2	93.4	1.46	1.47	16.21	16.75	14.77	15.73
66	42.5	Wall	0.66	57.08	57.59	7.24	8.78	91.2	92.7	1.47	1.48	16.56	16.76	15.18	15.65

TVS control

Case				T_{sensor} (°C)		x_{N_2} (%)		$x_{NOVEC_{1230}}$ (%)		ρ_{N_2} (kg m^{-3})		$\rho_{sat_{NOVEC_{1230}}}$ (kg m^{-3})		ρ_{ave} (kg m^{-3})	
$\mathcal{F}$	$\mathcal{P}_{h.l.}$	Method	$T_{profile}$	Min	Max	Min	Max	Min	Max	Min	Max	Min	Max	Min	Max
66	26	Coil	56	55.46	57.87	0.0	0.97	99.03	100.0	1.30	1.30	15.70	15.90	15.55	16.95
66	26	Coil	50	49.78	49.96	2.13	2.75	97.25	97.86	1.11	1.11	13.07	13.15	12.74	12.89
66	26	Coil	45	44.35	44.99	5.76	7.93	92.07	94.23	0.98	0.98	10.84	11.09	10.06	10.51
66	26	Coil	40.5	40.42	40.48	9.27	9.49	90.51	90.72	0.88	0.88	9.40	9.42	8.59	8.63

experiments. In addition, no extrapolation can be applied to the available data because of the well-known nonregular evolution of Henry's law constants.

Nonetheless, a characteristic time τ_{abs} can be associated to the absorption of nitrogen by the subcooled liquid, and a characteristic time τ_{cond} can also be associated to the condensation of the $NOVEC_{1230}$ vapor by this subcooled liquid. The average molar fraction evolution indicates that the subcooled liquid absorbs nitrogen gas faster than it condenses $NOVEC_{1230}$ vapor, thus $\tau_{abs} \ll \tau_{cond}$. With the thermal power ratio decrease, a thermal equilibrium tends to be established, and the nitrogen distribution tends to a new equilibrium state with an average nitrogen molar fraction of 9% in the ullage.

The effect of the subcooled jet on the nitrogen concentration stratification in the tank is quantified in Fig. 11, where several temperature distributions corresponding to an increasing time after the injection start are displayed on the left picture. The selected distributions correspond to given values of the average tank temperature $T_{ave} =:$ 56 °C, 50 °C, 45 °C, and 40.5 °C. The middle and right pictures of Fig. 11 display, respectively, the stratification of the molar fractions and the density profiles in the ullage for each of these selected times after the injection start. It can be observed that the subcooled jet absorbs the gaseous nitrogen in the ullage almost instantaneously, since 0.2 h after the injection start ($T_{ave} = 56.0\,°C$) the average nitrogen molar fraction is null. At a later time after the injection start, as the average temperature decreases in the tank ($t = 0.61$ h for $T_{ave} = 50.0\,°C$, $t = 1.23$ h for $T_{ave} = 45.0\,°C$, and $t = 4.66$ h for $T_{ave} = 40.5\,°C$), a thermal balance establishes inside the tank which induces an equilibrium distribution of the nitrogen fraction in the liquid bath and ullage of the tank. At the end of the experiment, a thermal equilibrium is reached, with the thermal power ratio equals to unity, and the nitrogen average molar fraction in the ullage reaches a plateau value of 9% as previously observed in Fig. 9.

The destratification effect of the subcooled jet is observed in Fig. 11 and Table 1, with vertical distributions of T, ρ, and x homogenized in the ullage after the injection start.

6 Conclusion

An analysis of the thermal stratification observed during self-pressurization and TVS control experiments in an on-ground experimental facility, using $NOVEC_{1230}$ as substituent fluid [5], has been presented. The presence of noncondensable gases, essentially nitrogen in the present case, has to be taken into account in order to explain the observed thermal stratification in the tank.

Assuming the ullage pressure to be independent of hydrostatic pressure and the $NOVEC_{1230}$ vapor to remain at saturation in the whole ullage, a stratified distribution of the ullage components molar fraction can be derived. This distribution is consistent with the expected nitrogen concentration associated with the $NOVEC_{1230}$ purification procedure and also satisfies a density stratification condition where the lighter fluid remains on top of the heavier one. Consequently, it seems convincing to explain the inverse thermal stratification observed in the experiments by this ullage nitrogen concentration stratification.

The total nitrogen mass present in the tank is divided into a first part dissolved in the liquid bath and a second part in gaseous state in the ullage. The distribution between those two parts, of the nitrogen total mass, depends on the tank thermal conditions.

During TVS control experiments, the subcooled jet injection induces a strong thermal imbalance in the tank right after the injection start, which leads in turn to the very fast dissolution of the nitrogen into the liquid bath. As the injection goes on, the thermal imbalance decreases and the nitrogen mass in gaseous phase in the ullage increases to reach a stabilized level once the thermal equilibrium is reached inside the tank.

The experimental data presented in this study should prove useful for the future validation of multiphase and multispecies numerical simulations of tank control experiments. The main limitation of the present experiments is the lack of control of the nitrogen fraction in the tank, which results from the substituent fluid purification procedure. The detailed influence of a known total mass of nitrogen on the inverse thermal stratification during SP experiments and the absorption dynamic during TVS control experiments requires to develop a new experimental setup in a smaller tank with a nitrogen quantity tuned using typically an iterative void pumping procedure such as presented in Ref. [11].

Acknowledgment

The authors acknowledge the joint support of the Centre National d'Etudes Spatiales (CNES) and Air Liquide Advanced Technologies (ALAT). The laboratory LEGI is part of the LabEx Tec 21 (Investissements d'Avenir—Grant Agreement No. ANR-11-LABX-0030).

Nomenclature

c_p = fluid massic specific heat (J kg^{-1} K^{-1})
$\mathcal{F}$ = tank liquid filling (%)
M = molar mass (kg m^{-1})
$\dot{m}_{inj}$ = injection mass flow rate (kg s^{-1})
p_{atm} = atmospheric pressure (Pa)
$p_{vap} = p_{tot}$ = experimental ullage pressure (Pa)
p_{N_2} = nitrogen partial pressure (Pa)
$p_{NOVEC_{1230}}$ = $NOVEC_{1230}$ partial pressure (Pa)
$\mathcal{P}_{h.l.}$ = tank heat load (W)
$\mathcal{P}_{jet}$ = jet cooling power (W)
R = ideal gas constant: 8.314 J mol^{-1} K^{-1}
T_{amb} = ambient temperature in the experimental room (°C)
T_{ave} = average temperature inside the tank (°C)
T_{env} = envelope temperature (°C)
T_{inj} = injection temperature (°C)
T_{sat} = saturation temperature (°C)
x = molar fraction (%)
$\Delta T_{h.l.}$ = wall thermal imbalance constant (°C)
ε = thermal accommodation factor of the active insulation technique (°C)
ρ = fluid density (kg m^{-3})

References

[1] Lin, C., Van Dresar, N. T., and Hasan, M., 1991, "A Pressure Control Analysis of Cryogenic Storage Systems," AIAA Paper No. 91-2405.
[2] Majumdar, A., Valenzuela, J., LeClair, A., and Moder, J., 2016, "Numerical Modeling of Self-Pressurization and Pressure Control by a Thermodynamic Vent System in a Cryogenic Tank," Cryogenics, **74**, pp. 113–122.
[3] Kassemi, M., and Kartuzova, O., 2016, "Effect of Interfacial Turbulence and Accommodation Coefficient on CFD Predictions of Pressurization and Pressure Control in Cryogenic Storage Tank," Cryogenics, **74**, pp. 138–153.
[4] Mer, S., Fernandez, D., Thibault, J.-P., and Corre, C., 2016, "Optimal Design of a Thermodynamic Vent System for Cryogenic Propellant Storage," Cryogenics, **80**, pp. 127–137.
[5] Mer, S., Thibault, J.-P., and Corre, C., 2016, "Active Insulation Technique Applied to the Experimental Analysis of a Thermodynamic Control System for Cryogenic Propellant Storage," ASME J. Therm. Sci. Eng. Appl., **8**(2), p. 021024.
[6] Hartwig, J., Chato, D., McQuillen, J., Vera, J., Kudlac, M., and Quinn, F., 2014, "Screen Channel Liquid Acquisition Device Outflow Tests in Liquid Hydrogen," Cryogenics, **64**, pp. 295–306.
[7] Barsi, S., and Kassemi, M., 2013, "Investigation of Tank Pressurization and Pressure Control—Part I: Experimental Study," ASME J. Therm. Sci. Eng. Appl., **5**(4), p. 041005.
[8] Demeure, L., 2013, "Comportement Thermodynamique de Réservoirs d'ergols Cryogéniques," Ph.D. thesis, Université de Grenoble, Grenoble, France.
[9] 3M, 2003, "Novec 1230™3M—Product Information," 3M, Maplewood, MN, Technical Report No. 98-0212-2667-9.
[10] Bullard, B., 1972, "Liquid Propellant Thermal Conditioning Test Program Final Report," Lockheed Missiles and Space Co., Sunnyvale, CA, NASA Report No. CR-72971.
[11] Barsi, S., 2011, "Ventless Pressure Control of Cryogenic Storage Tanks," Ph.D. thesis, Case Western Reserve University, Cleveland, OH.